Lensless passive and active microwave imaging on MAST

Plasma Phys. Control. Fusion **55** (2013) 124010 (6pp) doi:10.1088/0741-3335/55/12/124010

Lensless passive and active microwave imaging on MAST

S J Freethy[1], B K Huang[1,2], V F Shevchenko[1] and R G L Vann[3]

[1] EURATOM/CCFE Fusion Association, Culham Science Centre, Abingdon, Oxfordshire, UK
[2] Centre for Advanced Instrumentation, Department of Physics, Durham University, Durham, UK
[3] York Plasma Institute, Department of Physics, University of York, York, UK

E-mail: simon.freethy@ccfe.ac.uk

Received 29 June 2013, in final form 10 September 2013
Published 28 November 2013
Online at stacks.iop.org/PPCF/55/124010

Abstract
A novel microwave imaging system (SAMI) which utilizes an array of phase sensitive antennas to synthesize an optical aperture has been designed and deployed on MAST. The system requires no optical components for focusing and yet is able to image up to half of the plasma surface simultaneously. All image formation is done in post processing and SAMI can be refocused after the fact. SAMI is capable of imaging both passive thermal emission and scattered radiation from an active probing source simultaneously without compromising performance. We have used the diagnostic to observe highly anisotropic thermal emission characteristic of high β plasma devices which are overdense to regular ECE emission. This is an exciting emerging diagnostic field and we present our first observations here.

(Some figures may appear in colour only in the online journal)

1. Introduction

Thermal radiation in the microwave regime from conventional aspect-ratio fusion machines is concentrated around cyclotron harmonics due to the gyromotion of the electrons. This electron cyclotron emission (ECE) has been used as a diagnostic tool for decades [1]. In the presence of turbulent plasma structures, this information becomes multi-dimensional, requiring the ability to distinguish its spatial structure to maximize the diagnostic information available.

In high-β plasma devices however ECE is not typically observed due to the first few cyclotron harmonics being completely enclosed by the plasma density cut-off layers. However, thermal microwave emission is still present under these circumstances as emission from harmonics is propagated by the electrostatic Bernstein modes. These modes may couple to the vacuum modes via a double mode conversion (MC) process. First, the Bernstein mode couples to the electromagnetic X-mode in the region of the upper hybrid resonance (UHR) and then this X-mode to an O-mode in the region of the plasma density cut-off. The coupling efficiency of the X–O part of this double conversion process depends strongly on the projection of the wavevector to the magnetic field at the density cut-off [2, 3] and thus the observed emission is highly anisotropic with Bernstein emission (EBE) localized within two narrow angular MC cones.

EBE was first observed in fusion plasmas at the W7-AS stellarator [4] using a single horn radiometer at an oblique angle to the magnetic field and density surface. Shortly after, this emission was observed on COMPASS-D and MAST in a similar manner [5]. As the reciprocal process is used as a way to couple microwave power to overdense plasmas, study of the emission became more common, with the purpose of informing heating and current drive experiments. It was quickly realized that the emission carried with it a large amount of information on the plasma magnetic field structure. Experiments were designed to use the minima of the observed emission spectra's sawtooth like structure to provide constraints on the magnetic field [6]. The modelling in this case found that they could only fit the emission spectra minima by allowing a localized bump in the poloidal field near the separatrix [7]. NSTX also performed scans of the narrow angular cones characteristic of this emission using a single point approach with great success, allowing them to accurately measure the angle of peak emission over the course of many shots [8].

The angular position of the EBE provides an independent constraint on the magnetic field which allows one to measure the magnetic field pitch as a function of density, and thus

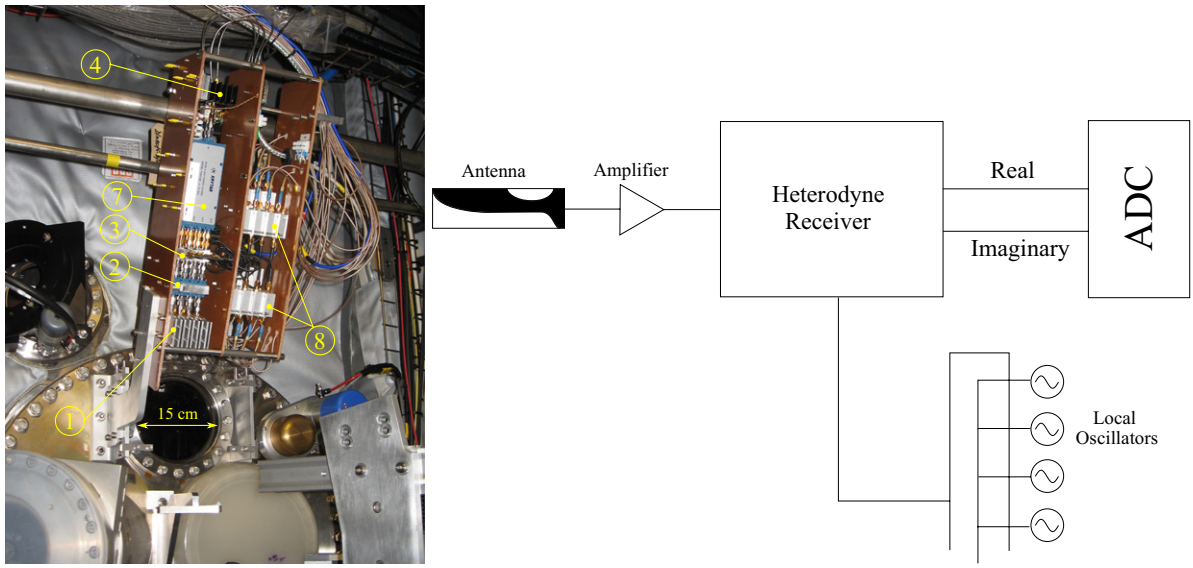

Figure 1. The SAMI system installed on MAST. The array (not shown) sits either looking into the 15 cm window shown situated 20 cm up from the midplane or on a window just underneath at the machine midplane.

with Thomson scattering measurements, radius. Recently this quantity was measured using a fast rotating mirror and multi-frequency radiometer [9]. The conclusion of the work was that, as for the spectral measurements, the data is best explained by a localized magnetic field bump near the separatrix.

Despite this, the field of EBW emission research is still in its infancy and there have not until now been any two-dimensional maps of the emission, or detailed study of how both MC cones behave in time. With the purpose of further investigating the subtleties of the MC process a synthetic aperture microwave imaging (SAMI) array was designed and built for MAST [10]. SAMI is able to resolve both angular cones in high time resolution (10–100 kHz) 2D maps of the emission process at 16 frequencies covering up to three emission harmonics. It represents a huge step forward in this emerging field and the refinement of the physical picture of this emission promises to contribute to RF heating and current drive as well as MHD stability.

An array of phase sensitive antennas are capable of forming images by scanning a pattern of constructive interference over the field of view, known as the beam forming or phased array technique. However, aperture synthesis arrays, unlike traditional beam formed arrays, can image the whole field of view simultaneously without the need for realtime beam steering. It is worth mentioning here that a SAMI array also requires no focusing optics at all and so eliminates the requirement for large single apertures or neutron sensitive lenses or mirrors making the techniques it utilizes an ideal choice for future fusion reactors.

Along with the passive imaging capabilities, SAMI has the ability to actively probe the plasma's reflective layers with a narrow band source. It can do this simultaneously without compromising the emission measurements. Measuring the Doppler shift of backscattered radiation from plasma density fluctuations allows the possibility of measuring rotation, which is important both for edge stability and transport [11].

2. Synthetic aperture imaging

The aperture synthesis technique, routinely used in radio astronomy, is based on the van Cittert–Zernike theorem [12, 13] which describes the propagation of spatial coherence. This theorem states that the complex visibility of a remote incoherent source is equal to the Fourier transform of the mutual coherence function.

$$\Gamma_{i,j} = \int G(\eta, \xi)\, I(\eta, \xi)\, \mathrm{e}^{\mathrm{i}k(u\eta + v\xi)}\, \mathrm{d}\eta\, \mathrm{d}\xi, \tag{1}$$

where u and v give the number of wavelengths between points i and j along Cartesian axes in the observation plane; $\xi = \sin\theta$ and $\eta = \cos\theta \sin\phi$ are direction coordinates of a point of the distant source; G represents the antenna gain pattern; I is the intensity of the source; and $\Gamma_{i,j}$ is the mutual coherence function of complex signals S_i and S_j measured at two points i and j in the plane of observation:

$$\Gamma_{i,j} = \int S_i(t)\, S_j^*(t - \tau)\, \mathrm{d}t. \tag{2}$$

Here the star denotes the complex conjugation and τ is the time lag between measurements at points i and j. In the special case of $\tau = 0$ the mutual coherence function is called the visibility function. The two important assumptions in the derivation of equation (1) are that the source is in the far field and that the source is spatially incoherent, i.e. that correlations of fields at different points on the emitting body are zero, $\langle E(r)E(r')\rangle = \delta(r - r')$. Equation (1) can be identified as a sample of the two-dimensional Fourier transform of the product of the intensity distribution and antenna gain pattern at a point in Fourier space (u, v). Knowing this, one can construct an array of antennas and measure the cross-correlations for each pair of antenna signals, thereby providing sampling of the Fourier transform of the image in front of the array. With a sufficient number of antenna pairs, one may perform an inverse

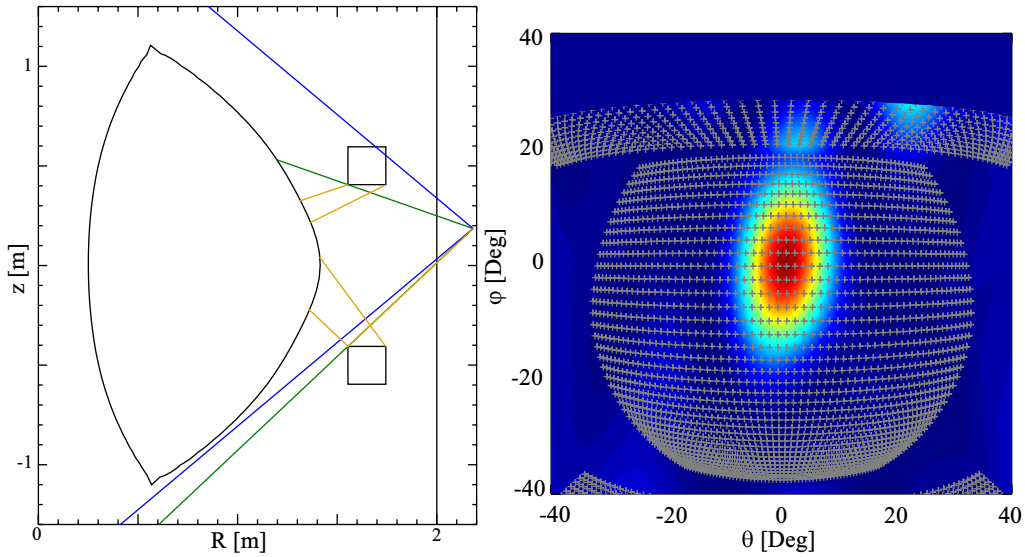

Figure 2. Left: the view of the plasma from the SAMI array in poloidal cross-section. Blue lines denote ±40°, green lines are the unobstructed field of view and orange lines denote the reflections from poloidal field coils. Right: the SAMI point spread function at 13 GHz in image coordinates. Over-plotted is the plasma density cut-off surface and upper and lower poloidal field coils.

Fourier transform to obtain an approximation to the real source brightness distribution. An excellent reference can be found in Thompson [14].

3. The SAMI system

SAMI is an array of phase sensitive antennas. Both real and imaginary parts of the electric field detected from each of these antennas are downconverted in frequency by a heterodyne receiver. SAMI is a very broadband system covering the range from 10–35.5 GHz in 16 steps (figure 1). The signals are then digitized by a 14 bit 250 MHz FPGA-controlled digitizer. Storing the downconverted electric fields and performing the image analysis offline provides great flexibility to account for possible non-ideal behaviour in the electronics and the ability to consider multiple image inversion algorithms. For more details on the design and construction of SAMI, we point the reader to a dedicated paper [10].

SAMI is a wide-field imaging device with a routine field of view of ±40°. Figure 2 (left) shows the view of the system in poloidal cross-section. The extreme upper section of the plasma is obscured by a poloidal field coil, but the majority of the plasma surface is visible. The image on the right of figure 2 shows the response of the system to a point source at 13 GHz in the centre of the field of view; the coordinates are the instruments viewing angles θ, ϕ used in equation (1). The figure is calculated by extrapolating the antenna electric fields, with zero relative phase, to the plasma density cut-off surface (over-plotted) for $z = -0.8$ to 0.5 m and a toroidal angle of ±30°. This extrapolation is done using a vector Huygens principle in combination with Shellkunoff equivalence principle [15]. Note the slightly elongated appearance of the point source response. This is a direct result of the asymmetric array shape chosen specifically to optimize a modified beam efficiency function to get the best performance [16]. There is a balance between beam sidelobe level and angular resolution which must be met and SAMI was optimized with both of these in mind. Higher frequencies show a narrower point source response in accordance with diffraction limitations.

SAMI is also equipped with the ability to actively probe the plasma with a wide angle source and measure the backscattered radiation power and Doppler shift over the whole surface. It does this simultaneously with its passive imaging without compromising the image quality. The Doppler part of the system was benchmarked in the lab by using a rotatable corner reflector placed in front of the diagnostic. The results can be seen in figure 3: the rotation of the reflector can be clearly identified near the centre of the image and this is repeated for each frequency channel with the Doppler shifted pattern growing smaller with increasing frequency. There are some irregular artefacts present in the Doppler map due to a spatial aliasing from the fact that only a small number of antennas is used. These can only be removed by adding more antennas to the array.

4. Plasma observations

SAMI has now gathered a database of plasma discharges and a wealth of 2D information about the anisotropic thermal emission from MAST. We nearly always see two well formed MC windows, which are well resolved by SAMI. These always have the correct inclination direction for the MAST magnetic field. Figure 4 (left) shows a predicted image for a low density L mode shot calculated by the analytic equation in given by Mjolhus [3] and convolved with the SAMI point source response. On the right is the measured image. The angular positions are well reproduced by SAMI, however the relative brightness is not well reproduced. There are no ray effects included in this model, only MC efficiency assuming a uniform background brightness temperature. This may account for the anomaly.

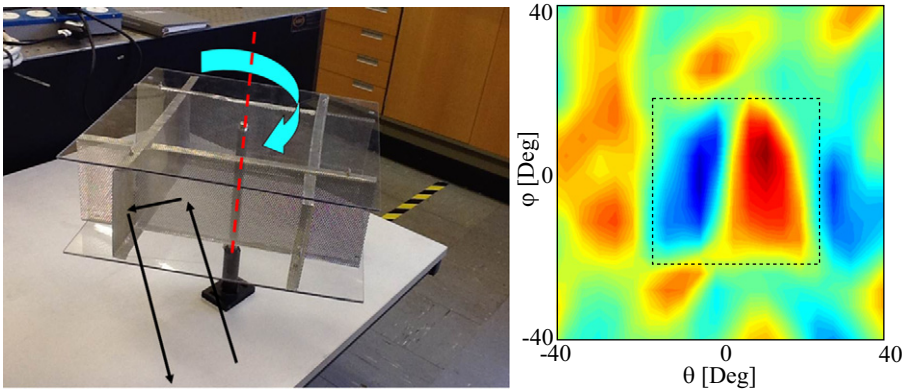

Figure 3. Left: Doppler back-reflected imaging in the lab was performed using a rotatable corner reflector. Right: After a 0.5 s acquisition we are able to reconstruct the velocity map at all frequencies. Red here represents positive Doppler shift (towards), Blue negative (away).

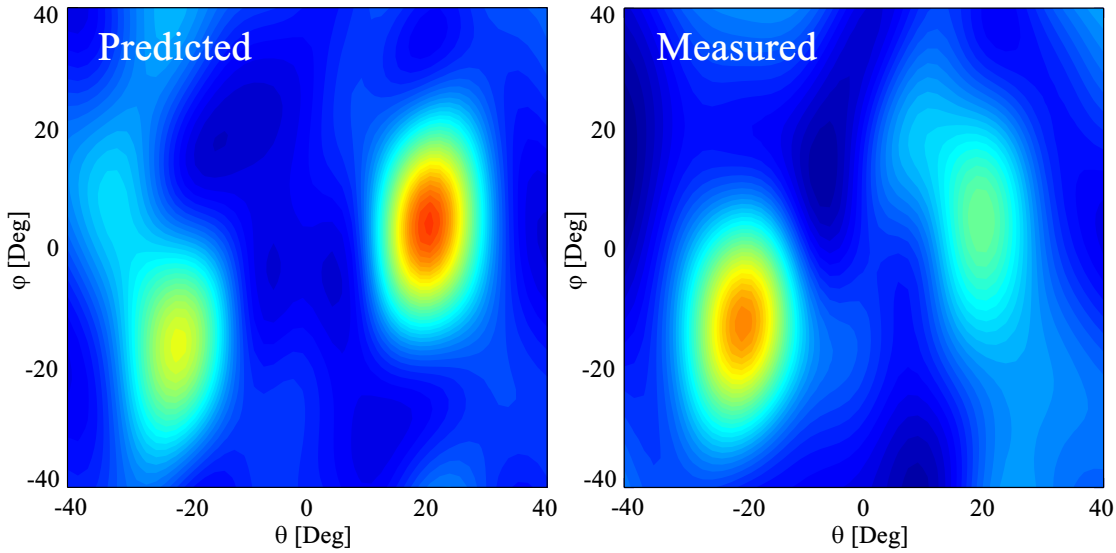

Figure 4. Left: the predicted MC efficiency calculated from the Mjolhus formula for 13 GHz [3] and convolved with the SAMI point source response. Right: the Fourier inversion for the intensity for the low density shot 27022 at 13 GHz: We can clearly identify two well formed and distinct MC windows with the correct inclination direction.

We also observe a density dependence of the emission power. This is the currently the topic of some debate within the community as to its explanation and is an area of active research because of its implications for magnetic field measurements using this technique. Figure 5 shows the spatially integrated power for a series of similar shots with differing line average density. The expected power from the first harmonic is plotted as a dashed line in arbitrary units, where we have used a simple 1D model described in [6]. The predicted spectral minima at 20.5 GHz is observed for the low density case, however significant deviation from the expected power can be seen (black curve) for frequencies between 10 and 16 GHz. Furthermore as we increase the line averaged density, we see the observed power fall at all frequencies, with the spectral peak moving to higher frequencies. There is little change in the expected spectrum for each of these shots. The lowest peak power is a factor of 10 lower than the highest. This suppression has consequences for electron Bernstein heating and current drive and may affect pitch angle measurements if it is spatially distributed.

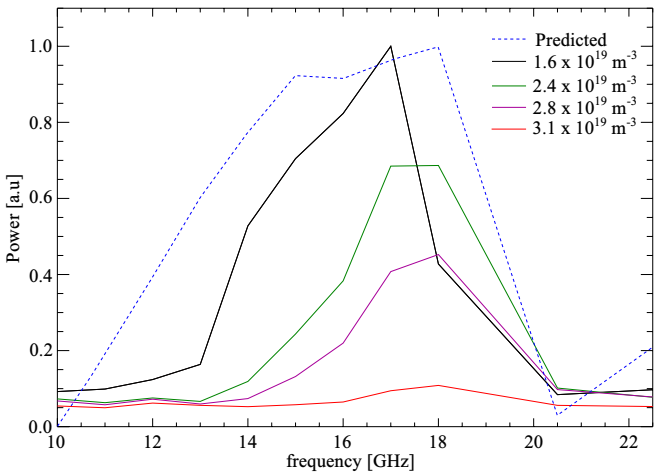

Figure 5. The relative power measured by SAMI around the first harmonic for L mode shots of differing density. We see that the power is damped first and most strongly at lower frequencies. The peak power in the lowest density shot is a factor of 10 higher than the highest density shot.

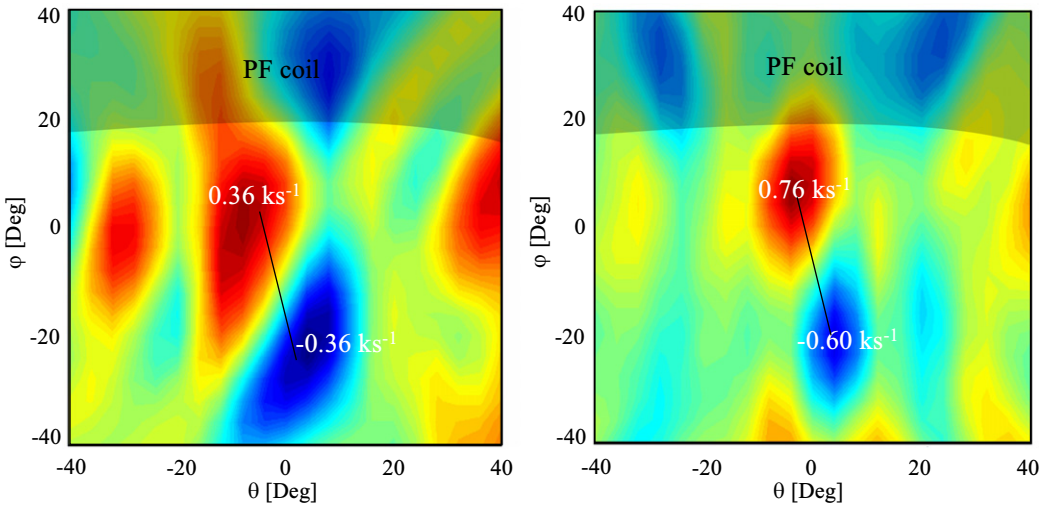

Figure 6. Left: a 2D Doppler shift map for 13 GHz integrated over 10 ms. The colour represents the centre of gravity of the backscattered/reflected radiation spectrum, just as in figure 3. Red is positive, blue is negative. Here SAMI is positioned 20 cm above the midplane so the shaded region represents the poloidal field coil obstruction. The plasma density cut-off is similar to that shown in figure 2. Right: the same, but this time for 16 GHz; this corresponds to a deeper plasma layer. The rotation appears to have changed pitch.

The active probing part of the system also performs well. Figure 6 shows two 2D Doppler shift maps. The first is at 13 GHz and the second is at 16 GHz representing reflection from deeper within the plasma. The colour represents the centre of gravity of the detected frequency spectrum for that particular direction, Red is positive and blue is negative. At this point we remind the reader of the point spread function shown in figure 2. The real Doppler map is convolved with this, which places a limit on the minimum resolvable size of a structure. We can see that the observed rotation is inclined in a direction perpendicular to that of the magnetic field as shown by the black line. The map for 13 GHz appears to show a slightly different inclination to that predicted. We observe this spatial structure in the Doppler shift as the received Doppler shifted radiation is predominantly composed of Bragg backscattered radiation from plasma turbulent structures aligned along the magnetic field. Thus the magnitude of the Doppler shift tells us about the projection of the turbulent total velocity perpendicular to the magnetic field [17].

If we now look at the evolution of the Doppler shift in time, selecting the direction of maximal shift for both frequencies we can see an acceleration from 20 ms onwards. The plasma layer at 16 GHz can be see to produce a higher Doppler shift than at 13 GHz illustrating a faster rotation of this plasma layer (figure 7).

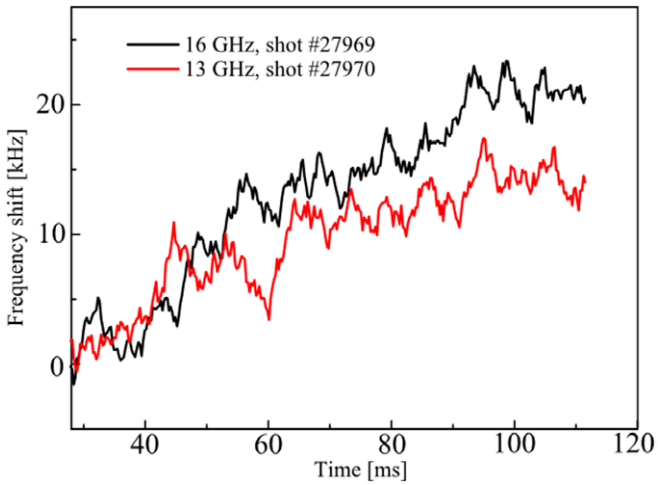

Figure 7. Examining the maximum Doppler shift as a function of time for 13 and 16 GHz. 16 GHz is reflected from deeper within the plasma. We can see that 16 GHz accelerated to a higher velocity than 13 GHz.

5. Conclusions

A synthetic aperture imaging array has been designed built and deployed on MAST which is capable of passively observing thermally emitted radiation and imaging Doppler shifted backscattered radiation from an active probing source simultaneously. We have provided the first images of the predicted anisotropic emission from plasma devices where the cyclotron harmonics are completely obscured by the plasma density cut-off, a direct result of a double mode conversion process. Theoretical predictions for a plasma slab predict the mode conversion to be aligned along magnetic field lines and can be used to infer high resolution magnetic pitch profiles. We have obtained good agreement with the theoretically predicted angles of the EBE for low density L mode at 13 GHz, although the relative brightness is not accurately predicted. A more accurate treatment of the Bernstein wave radiative transfer in the bulk plasma needs to be carried out.

We have also observed a dependence of the emission spectrum to the average plasma density. Plasmas with densities above $1.6 \times 10^{19}\,\mathrm{m}^{-3}$ have been shown to have strongly suppressed spectra with the spectral peak moving to higher frequencies.

We have also provided the first 2D maps of Doppler shift from an active probing source, demonstrating the ability of the diagnostic to measure Doppler shifted radiation which

corresponds qualitatively with what we expect, demonstrating a speed up of the plasma rotation in the early stages of a plasma's development.

Acknowledgments

This work was funded partly by EPSRC under grant EP/H016732, by the University of York, by the RCUK Energy Programme under grant EP/I501045 and the European Communities under the contract of Association between EURATOM and CCFE. The views and opinions expressed herein do not necessarily reflect those of the European Commission.

References

[1] Park H *et al* 2003 Recent advancements in microwave imaging plasma diagnostics *Rev. Sci. Instrum.* **74** 4239–62

[2] Prienhaelter J and Kopecký V 1973 Penatration of high-frequency waves into a weakly inhomogeneous magnetized plasma at oblique incidence and their transformation to Bernstein modes *J. Plasma Phys.* **10** 1–12

[3] Mjølhus E 1984 Coupling to Z mode near critical angle *J. Plasma Phys.* **31** 7–28

[4] Laqua H P *et al* 1998 Electron Bernstein wave emission from an overdense plasma at the W7-AS stellarator *Phys. Rev. Lett.* **81** 2060–3

[5] Shevchenko V *et al* EBW emission observations on COMPASS-D and MAST *28th EPS Conf. on Controlled Fusion and Plasma Physics* pp 1285–9

[6] Shevchenko V 2000 ECE measurements via B–X–O mode conversion: a proposal to diagnose the q profile in spherical tokamaks *Plasma Phys. Rep.* **26** 1000–4

[7] Preinhalter J *et al* EBW simulation for MAST and NSTX experiments *AIP Conf. Proc.* **787** 349–52

[8] Diem S J *et al* 2009 Investigation of electron Bernstein wave EBW coupling and its critical dependence on EBW collisional loss in high-β, H-mode ST plasmas *Nucl. Fusion* **49** 095027

[9] Shevchenko V F *et al* 2011 Two dimensional studies of electron Bernstein wave emission in MAST *Fusion Sci. Technol.* **59** 663–9

[10] Shevchenko V F *et al* 2012 Synthetic aperture microwave imaging with active probing for fusion plasma diagnostics *J. Instrum.* **7** P10016

[11] Hillesheim J C *et al* 2009 A multichannel, frequency-modulated, tunable Doppler backscattering and reflectometry system *Rev. Sci. Instrum.* **80** 083507

[12] van Cittert P H 1934 Die wahrscheinliche schwingungsverteilung in einer von einer lichtquelle direkt oder mittels einer linse beleuchteten ebene *Physica* **1** 201–10

[13] Zernike F 1938 The concept of degree of coherence and its application to optical problems *Physica* **5** 785–95

[14] Thompson A R, Moran J M and Swenson G W Jr 2004 *Interferometry and Synthesis in Radio Astronomy* (Weinheim: Wiley)

[15] Schelkunoff S A 1939 Some equivalence theorems of electromagnetics and their application to radiation problems *Bell Syst. Tech. J.* **15** 92–112

[16] Freethy S J *et al* 2012 Optimization of wide field interferometric arrays via simulated annealing of a beam efficiency function *IEEE Trans. on Antennas Propag.* **60** 5442–6

[17] Truc A, Honoré C, Hennequin P and Quéméneur A, Quasi-optical gaussian beam tracing to evaluate doppler backscattering conditions *Nucl. Fusion* **46** S809